




Research Article

Pressure fluctuation of steam on the disc in a triple eccentric butterfly valve

Wang Haimin^{1,2}  · Hu Feng¹ · Kong Xiangshuai¹ · Chen Si¹

Received: 27 January 2020 / Accepted: 29 May 2020 / Published online: 10 June 2020
© Springer Nature Switzerland AG 2020

Abstract

The triple eccentric butterfly valve has an excellent structure for sealing fluid and can also produce additional torque to assist in opening or closing the valve. However, flow separation and vortex shedding often occur because of the rugged surface of the valve disc. Pressure fluctuation on the disc induces vibration and can severely damage the valve and pipeline. To investigate the pressure fluctuations due to steam, the CFD method is used to simulate the 3D unsteady flow inside the valve and to obtain the transient pressure and velocity at key points in the five typical sections in the fully open state. The discrete Fourier transform method is adopted to analyze the spectrum parameters. The Strouhal numbers for vortex shedding are also obtained. Finally, an experimental modal analysis is conducted to test the natural frequency of the disc–stem assembly. The tested natural frequency is much higher than the highest steam pressure fluctuation frequency in the case of the maximum flow rate. Moreover, pressure fluctuations caused by fluid force do not induce resonance of the disc–stem assembly and there no lock-in phenomenon occurs.

Keywords Pressure fluctuation · Triple eccentric butterfly valve · Disc–stem assembly · High-temperature steam

List of symbols

Main symbols

Re	Reynolds number
P	Static pressure
t	Time
P_{max}	Maximum static pressure
f	Main frequency of pressure fluctuation
f_s	Vortex shedding frequency
T_{in}	Inlet temperature
Q_m	Mass flow rate
V_{in}	Inlet velocity
P_{out}	Outlet pressure
x_n	A sequence of transient pressure in DFT
X_k	Discrete Fourier transform coefficients
Sr	Strouhal number
l	Geometric characteristic dimension
v	Inflow velocity of steam

Greek symbols

ρ	Density of steam
ξ	Valve resistance coefficient

Abbreviations

CFD	Computational fluid dynamics
DFT	Discrete Fourier transform
FFT	Fast Fourier transform

1 Introduction

In order to switch a butterfly valve more easily and improve its sealing performance, the valve disc is designed with a special triple-eccentric structure. This feature causes the valve stem installation position to form a large bump on one side of the disc. When fluid flows through the disc–stem assembly, the fluid pressure on both sides is not equal, leading to flow separation or vortex shedding.

✉ Wang Haimin, hmwang@usst.edu.cn | ¹School of Energy and Power Engineering, University of Shanghai for Science and Technology, Shanghai 200093, China. ²Shanghai Key Laboratory of Multiphase Flow and Heat Transfer in Power Engineering, Shanghai 200093, China.



Therefore, fluid pressure close to the wall of disc produces fluctuations which generate alternating forces and induce structural vibration.

The studied triple-eccentric butterfly valve is used in this work to control high-temperature steam discharge and should be opened quickly in order to deliver high-pressure and high-temperature steam to push a heavy load. If the flow control fails, the high-temperature steam-induced vibration causes the following adverse effects: (1) two sealing surfaces above and below the stem are worn; (2) the circle sealing surface in the disc is damaged; (3) the drive engagement surfaces of valve actuators are worn or fail; (4) the actuator misjudges the position signal of the disc; (5) vibration of the whole pipeline system worsens.

Therefore, it is necessary to study flow-induced vibration characteristics, analyze the steam pressure fluctuation frequency, and prevent resonance to reduce damage to structural components and the pipeline system [1, 2]. From the point of view of fluid dynamics, the steam flowing through the disc–stem assembly of a butterfly valve is an external flow problem, and vortex-induced vibration caused by fluid separation is a common phenomenon. Jauvtis [3] studied the effect of two degrees of freedom on vortex-induced vibration at low mass with damping. Govardhan [4] revealed the effect of the Reynolds number using controlled damping on the vortex-induced vibration and many similar studies are also available from [5–9] and so on. There are many methods of studying the frequency of pressure fluctuations. The lift coefficient is often used to study the flow around a cylinder. Govardhan [10] investigated the modes of vortex formation and frequency response of a freely vibrating cylinder. Khalak and Williamson [11] and Shoshani [12] conducted deterministic and stochastic analyses of the lock-in phenomenon in vortex-induced vibrations.

However, inside the valve passage, the flow is restricted to a smaller space between the disc and the seat. In this limited space, the pressure fluctuations are more complicated. Domnick [13], Galbally [14], Kumagai [15], Potter [16] and Youn [17] have studied the internal flow of fluid machinery and valves and found that the pressure fluctuations caused by unsteady flows can cause serious damage. Disc–stem vibration reduces the service life of components.

The mentioned previous studies mostly focused on the consequences of flow-induced vibration rather than on the frequency characteristics of fluid forces in valves. In this work, the velocity and pressure distributions of high-temperature steam (250 °C, 4.2 MPa, saturated steam) in the whole passage are studied for a triple-eccentric butterfly valve in the fully open state. In our previous work, Wang [18] have studied the external and integral vibration characteristics of a triple-eccentric butterfly valve. However,

it is difficult to study the induced vibration caused by the interaction between the disc and fluid using only empirical test methods because the fluid parameters inside the valve are so complicated. Therefore, the CFD method is used to study the high-pressure and high-temperature steam-induced vibration in a triple-butterfly valve. The steam pressure fluctuation characteristics near the wall of the disc are also studied based on the numerical simulation results. The natural frequency of the disc–stem assembly is tested through the experimental modal analysis method to determine the vibration frequency characteristics of various orders and to explore whether a lock-in frequency arises.

2 Computational methods and results

2.1 Geometry model

Figure 1 shows the 3D drawing of a valve disc–stem assembly, the diameter of valve disc is $\phi 400$ mm, the diameter of the stem is $\phi 62$ mm, and the maximum height of the eccentric bump is 88 mm. The total thickness of disc plus the height of bump is 133 mm. Because steam-induced vibration occurs mainly near the disc and its downstream area, to ensure that turbulence is fully developed during numerical simulation process, the outlet pipe is properly extended. The diameter of flow passage is $\phi 400$ mm, and the length of inlet pipe, which is the distance from inlet to the center of the stem, is also 400 mm, and the total length of fluid domain for is 1600 mm.

Referring to the structure of the triple-eccentric valve disc shown in Fig. 1, these two bumps are symmetrical about the axis of disc, therefore, the flow field of upper and lower parts is similar, just focus on upper half part. To obtain more detailed flow field information, the upper half was divided into five sections along the radial direction, which were ranked 0, 1, 2, 3, and 4, of which Section 0 was the central section of the whole flow domain. These sections and steam flow direction were shown in Fig. 2.

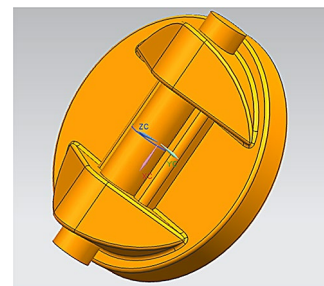


Fig. 1 3D view of stem–disc graphics of triple-eccentric butterfly valve

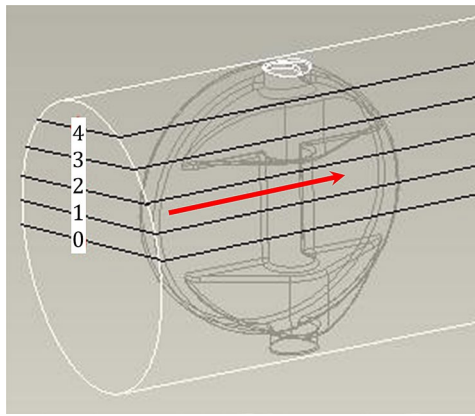


Fig. 2 Five selected radial sections and steam flow direction

Proper grid refinement and mesh quality should be performed and confirmed through mesh independency and $Y+$ criteria. Because the structure of disc–stem assembly is very complicated, the quality of the meshes near the disc should be comparatively higher through refinement, especially near the curved surfaces and other edges and corners. In addition, at the trailing edges of the disc–stem assembly, where vortex shedding can occur easily, the meshes here should be refined too.

Three sets of meshes with total grid numbers of 1.709, 2.366, and 3.204 million respectively, were performed in the simulations to verify mesh independence. The mesh sizes near the wall of disc are especially refined for boundary layers and possible separations. Three points (0,1200,0), (0,1200,90) and (0,1200,180) were selected as monitoring points. The results were shown that there was no noticeable difference in flow field (less than 3% difference in pressure and velocity of selected points in the flow field) at above three points. Considering computational time cost, the mesh with 1.709 million cells was chosen in this work.

The mesh quality was also checked, and the spacing of the first cell near the valve disc was set at 0.003 mm, and the overall non-dimensional wall distance $Y+$ in the valve was kept below 6.6.

2.2 Boundary conditions

The velocity inlet and the pressure outlet were applied to the boundaries of the flow passage. Table 1 provides four different operating conditions for the numerical simulation corresponding to different inlet velocities. According to the engineering application, the outlet pressures were all set as 4.0 MPa. The inlet temperature was $T_{in} = 250$ °C, the kinematic viscosity of 250 °C saturated steam was 0.807×10^{-6} m²/s, and its density was 21.86 kg/m³. The other parameters were set as in Table 1.

Table 1 Boundary conditions for different Cases

Case	Mass flow rate Q_m (kg/s)	Inlet velocity V_{in} (m/s)	Re	Outlet Pressure P_{out} (MPa)
1	50	18.10	2.98×10^6	4.0
2	100	36.42	6.00×10^6	4.0
3	150	54.63	9.00×10^6	4.0
4	200	72.84	1.20×10^7	4.0

2.3 Numerical methods

The commercial CFD software fluent is used as the solver. The pressure and velocity discretization are both use default settings. For the present study which both high and low Re regions are subjects of interest, the k - ω SST turbulence model and PISO algorithm are used to solve the control equations.

Time step can be a dominant factor in the simulation of pressure fluctuation of steam in a valve. Since the estimated main frequency of pressure fluctuation is below 200 Hz, even if the maximum frequency is extended to 1000 Hz, it is appropriate to choose a time step of 0.1 ms (1.0×10^{-4} s). This time step may not miss flow details, and also could not significantly increase computational run time. Therefore, this time step was used for the simulations reported in the following results.

In order to verify the validity of the numerical simulation method, a parameter of resistance coefficient ξ was introduced:

$$\xi = \frac{\Delta p}{\frac{1}{2} \rho V_{in}^2} \quad (1)$$

where Δp is pressure loss between inlet and outlet, and the denominator $\frac{1}{2} \rho V_{in}^2$ is dynamic pressure of inlet steam. Several tested data during operation was selected to compare with the numerical simulation results, these two groups of curves are obtained and shown in Fig. 3.

It can be observed that ξ obtained from CFD was very close to the experimental results, and the error is less than 5%. It means that the pressure field inner the valve obtained by numerical simulation is reliable.

2.4 Steam pressure fluctuation inner the valve

All four cases in Table 1 have been simulated, here the maximum flow rate which is corresponding to Case 4 is selected to analyze. Based on the numerical simulation results, the transient pressure distribution of

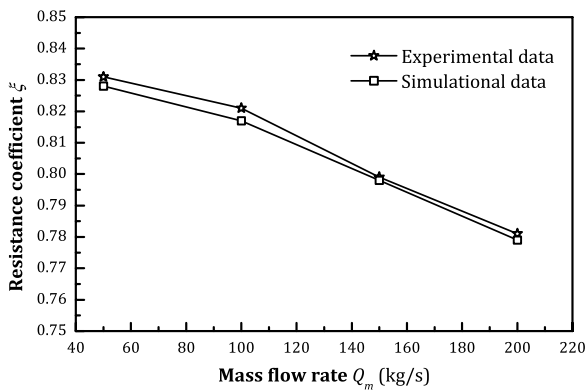


Fig. 3 Simulational resistance coefficient ξ compared with experimental results

high-temperature steam for the Section 0 to Section 4 in the passage are shown in Fig. 4a–e.

Of the five sections, the most intensive distribution of pressure contour was located at the outer edge of the bump in Section 0. Correspondingly, its curvature was the largest. This indicates that the pressure gradient here was the largest. From Section 0 to Section 4, the surface curvature of the solid wall decreased gradually and the pressure gradient close to the bump decreased as well. Furthermore, in Section 4, the pressure gradient on the flat back side of the disc increased significantly owing to the restriction of flow, the flow separation of the steam at the trailing edge of the disc led to a change of the pressure

gradient in the downstream region more obvious than in the other sections.

Studying the dynamics characteristics of pressure fluctuations is of great importance for analyzing the fluid forces acting on the disc. In order to monitor the steam pressure fluctuation inside the triple eccentric butterfly valves, many key points in the fluid field close to the disc–stem assembly were selected as shown in Fig. 5a–e.

According to the shape of the cross sections for the disc–stem assembly in Fig. 2 and the pressure distribution in Fig. 4, the shape of Sections 0 and 1 as well as Sections 2 and 3 are very similar in terms of the disc–stem assembly. For the convenience of research, of all five sections, only Section 0, Section 2, and Section 4 were selected to analyze the characteristics of pressure fluctuation.

In each section, 10 points close to the disc stem assembly in the fluid domain are selected to study their pressure fluctuations. Points 1 to 9 are on the bump side and Point 10 are on the other side of the disc–stem assembly, as shown in Fig. 5.

1. Pressure fluctuation at maximum flow rate

Of all four cases in Table 1, Case 4 has the maximum flow rate of steam and is selected as sample for exploring the pressure fluctuations from all numerical simulation results. Because the distribution of pressure in Fig. 4 varies dramatically at Points 2, 4, 6, 8, and 10 in each section, transient characteristics analysis was conducted for

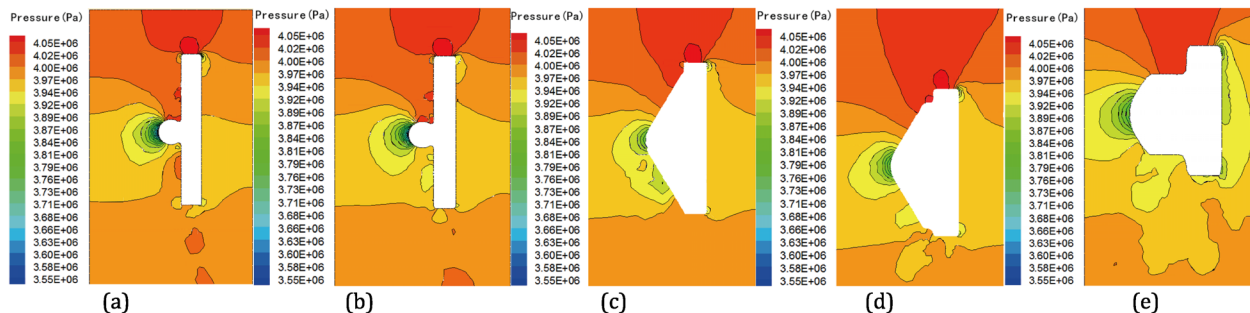


Fig. 4 Simulation results of pressure in five sections of valve for Case 4: **a** Section 0; **b** Section 1; **c** Section 2; **d** Section 3; and **e** Section 4

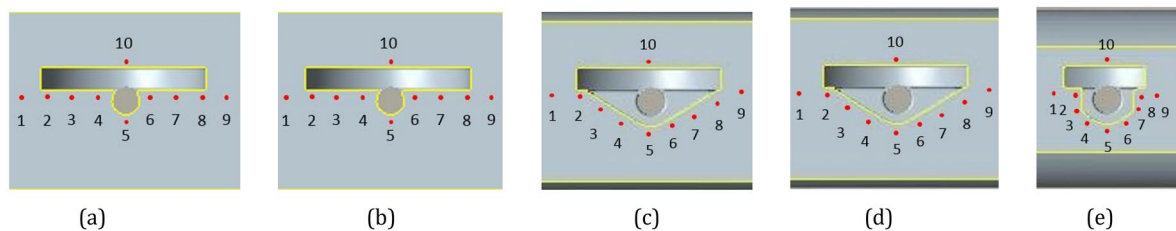


Fig. 5 Locations of monitoring points in five sections: **a** Section 0; **b** Section 1; **c** Section 2; **d** Section 3; and **e** Section 4

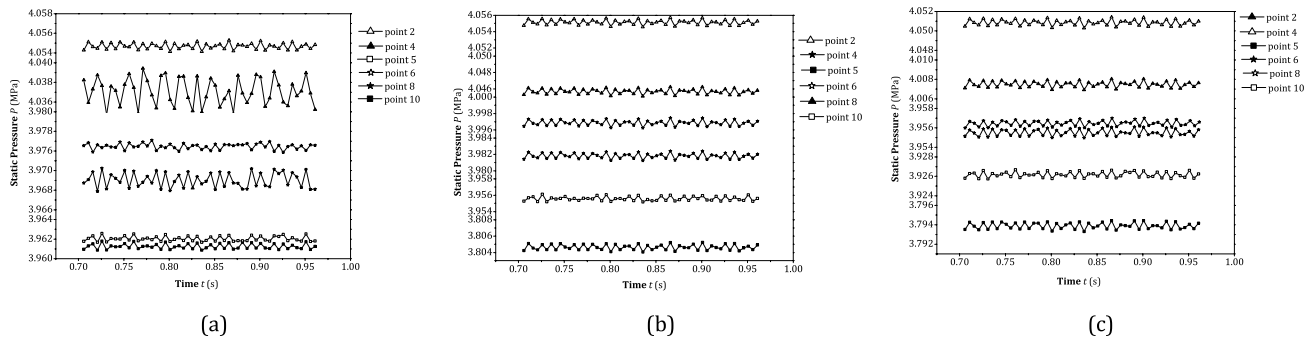


Fig. 6 Simulation results of transient pressure in three sections: **a** Section 0; **b** Section 2; and **c** Section 4

Points 2, 4, 5, 6, 8, and 10 in Sections 0, 2, and 4. Figure 6 shows a series of transient pressures in the time domain for each monitored point.

Section 0 featured the most intense pressure fluctuations for all six monitored points. In Fig. 6a, the maximum amplitude of pressure fluctuation was located at Point 4. Along the steam flow direction, the average pressures at Points 2, 4, 6, and 8 gradually decrease; but because Point 5 is located at the throat of the contraction section, the flow area decreases and the flow velocity increases, resulting in a lower average pressure than that at Points 4 and 6. The cross-sectional area at Point 10 was smaller than that at Point 5, so its average pressure was the lowest.

In Sections 2 and 4, the amplitudes of pressure fluctuations at each monitored point were similar because the cross-sectional area at Point 5 decreased obviously and was smaller than that of Point 10. Therefore, the average pressure fluctuation at Point 5 was smaller than that at Point 10 and was the lowest of all these points, just as shown in Fig. 6b, c.

To reveal pressure fluctuation frequency, a common method is discrete Fourier transform (DFT). It takes a sequence of sampled data (a signal), and computes the frequency content of that sampled data sequence. This will give the representation of the signal in the frequency domain, as opposed to the familiar time domain representation. This can be a very powerful tool in signal processing applications, because it allows one to examine any given signal in the frequency domain, which provides the spectral content of a given signal.

The DFT equation requires that every single sample in the frequency domain has a contribution from each and every one of the time domain samples. By computing the DFT coefficients X_k , it is performing a correlation, or trying to match the input signal to each of these frequencies. The magnitude DFT output coefficients X_k represent the degree of match of the time domain signal x_n to each frequency component.

A smart way to compute the DFT in a more efficient way is the FFT (fast Fourier transform). Rather than requiring N^2 complex multiplies and additions, the FFT requires $N \cdot \log_2 N$ complex multiplies and additions.

In this work, the function FFT(x) in MATLAB is used for transforming vector x. For matrices, the FFT operation is applied to each column. For length N input vector x, the DFT is a length N vector X, with elements X_k .

$$X_k = \sum_{n=1}^N x_n e^{-j2\pi(k-1)(n-1)/N}, \quad 1 \leq k \leq N \tag{2}$$

where x_n is from simulation data of transient pressure in time domain. By calculating the amplitude of X_k after FFT, the corresponding frequency spectrum between frequency and amplitude can be established according to the frequency series obtained from sampling period.

a. The frequency spectrum at key points

A series of key points such as Points 2, 4, 6, 8, and 10 located at Sections 0, 2, and 4 were selected for further study. The DFT method was then used to obtain their frequency spectrums. The results are displayed in Fig. 7., where two abscissa represent the monitoring points and frequency respectively and the ordinate represents the amplitude, that is, the modulus of coefficients X_k after applying the Fourier transform. The ordinate also represents the intensity of pressure fluctuations. Table 2 lists the main frequencies of all key points.

According to Fig. 7a and Table 2, at Section 0, except for the main frequency of Point 4 (54.7 Hz) and Point 6 (103.5 Hz), all the other main frequencies were 117.2 Hz. The amplitude of the Fourier transformation represents the proportion and intensity of different frequencies; Fig. 7a shows the highest amplitude at Point 4, whose amplitude was 786, and the amplitude of Point 8 was 408. Of these five points along Section 0, the amplitude of Point 8 was only smaller than the amplitude of Point 4.

Fig. 7 Transient pressure fluctuation frequency of points at three sections: **a** Section 0; **b** Section 2; and **c** Section 4

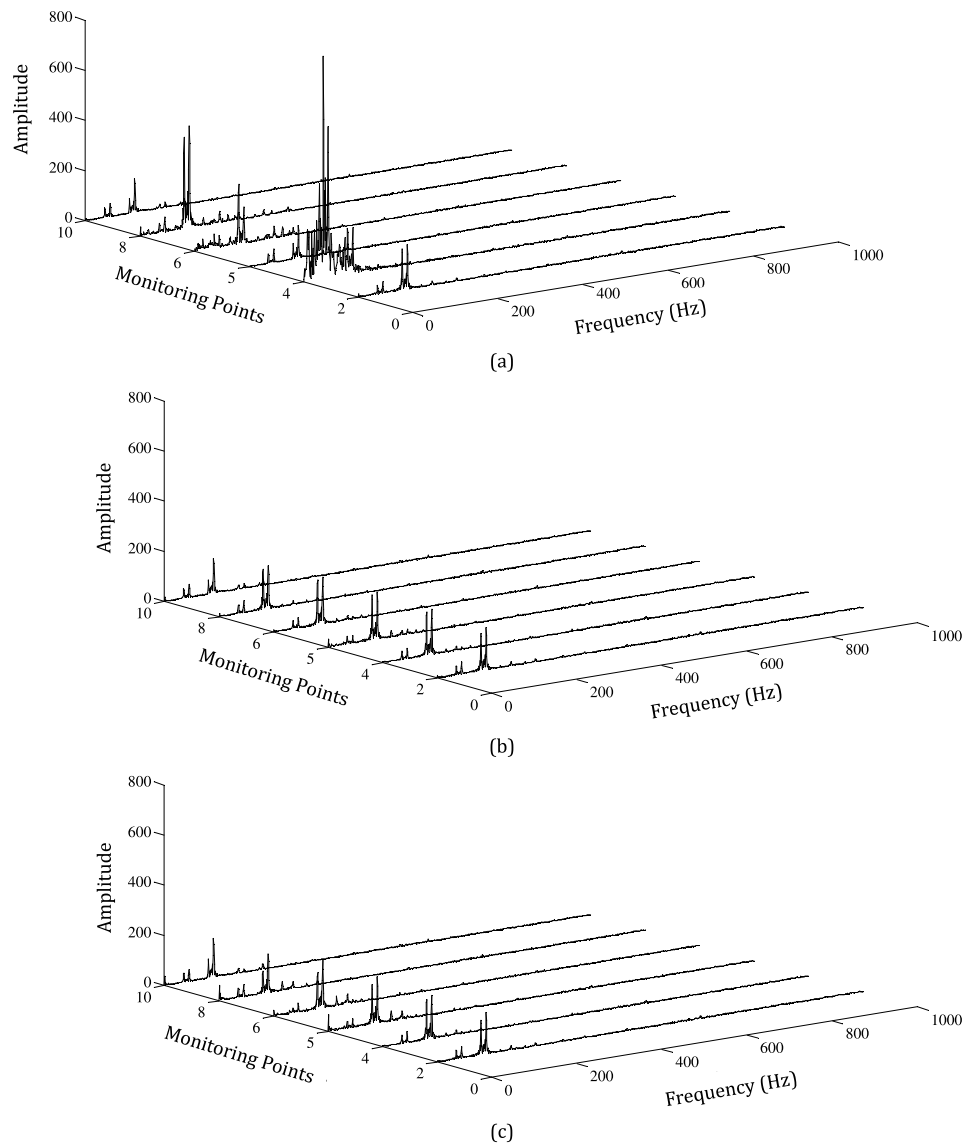


Table 2 The main frequency of pressure fluctuations for Case 4 (maximum flow rate)

Monitoring points	Main frequency f (Hz)		
	Sections		
	0	2	4
2	117.2	117.2	117.2
4	54.7*	117.2	117.2
5	117.2	117.2	117.2
6	103.5*	117.2	117.2
8	117.2	117.2	117.2
10	117.2	117.2	117.2

The amplitudes of Points 2, 5, 6, and 10 were 176, 131, 237, and 136, respectively. In addition to the main frequency, the secondary main frequency also appeared in the spectrum diagram. The secondary main frequency at Point 4 of Section 0 was 117.2 Hz, its amplitude was 118; the secondary main frequency at Point 6 was 117.2 Hz, its amplitude was 144. The secondary main frequencies at other points of Section 0 were all 103.5 Hz.

The results listed in Table 2 also indicate that the main frequency at all points of Sections 2 and 4 were the same at 117.2 Hz. According to Fig. 7b and c, the amplitudes of the same sections were basically identical. The amplitudes of the main frequency at Section 2 were 170, 182, 188, 187, 171, and 140, respectively from Point 2 to Point 10. The amplitudes of the main frequency at Section 4 were

166, 173, 184, 192, 154, and 155, respectively, from Point 2 to Point 10.

The main cause of pressure fluctuations at these key points may be the complex geometry of the disc-stem assembly. When the steam flows through the rugged surface, the pressure varies dramatically. On the core Section 0 of the passage, there are four right-angle turns in the disc-stem assembly, which force the steam flow direction to change significantly many times. Furthermore, the flow routes of steam is the longest of all sections, which leads to a more obvious pressure fluctuations at all points in Section 0. Especially at points 4 and 6, the vortex generated by flow separation at the right-angle turns may caused the fluctuation of the main frequency of pressure to be lower than that at other points. Comparing with Point 4, Point 6 is located downstream of the stem, and here the vorticity may be more stronger, so the pressure fluctuation frequency at Point 6 was higher than that at Point 4.

Along the flow direction, the bumps fixing the stem at Sections 2 and 4 were both trimmed by a circular arc transition and their flow routes became shorter as well. Therefore, the influence of the solid wall on the fluid was relatively weak when the steam flowed around the disc. Hence, in Figs. 6b, 7b, 6c, and 7c, the amplitudes of pressure fluctuation for all points in these two sections were relatively smaller.

b. Pressure fluctuation at Section 0

To explore the pressure fluctuation of steam close to the disc under different operating conditions, the transient pressures at different section conditions were calculated. According to the above analysis, pressure fluctuation at the monitoring points in Section 0 themselves fluctuated dramatically. Section 0 is selected here to study the pressure fluctuation for different flow rates, especially at Points 4, 5, and 8 as key points. The results are listed in Table 3.

Table 3 describes the calculation results for pressure fluctuation and main frequency at the monitoring points for four operating conditions at Section 0. From Case 1 to Case 4, the main frequency of pressure fluctuations at each point increased with increasing inlet flow rate.

Figure 8 shows the frequency spectrum of pressure fluctuation at different inlet flow rates at Section 0. The amplitude at Points 4, 5, and 8 gradually increased with increasing inlet flow rate while the magnitudes of the main frequency in Cases 3 and 4 alone exhibited little difference.

c. Strouhal number for the disc–stem assembly

By extracting the data for transient pressure of steam flowing inside the valve and calculating the variation of lift coefficient, the vortex shedding frequency can be

Table 3 Main frequency at Section 0 for Case 1 to Case 4

Case	Monitoring points	Main frequency f (Hz)
1	4	31.2
	5	31.2
	8	31.2
2	4	27.3
	5	58.6
	8	58.6
3	4	42.9
	5	85.9
	8	85.9
4	4	54.7
	5	117.2
	8	117.2

obtained for each case. This shedding frequency is related to object shape, inflow velocity, and geometric characteristic dimension. The relationship of these parameters is defined by the following formula:

$$f_s = Sr \frac{v}{l} \quad (3)$$

where f_s represents the vortex shedding frequency, Sr represents the Strouhal number, v represents the inflow velocity of fluid, and l represents the geometric characteristic dimension. When the valve was fully opened, the maximum thickness of valve disc was defined as the geometric characteristic dimension, and its value was $l = 133$ mm. The calculated Strouhal numbers for all four cases are listed in Table 4.

Even the inflow velocity and Reynolds numbers are clearly different while the dimensionless Strouhal numbers were extremely close, varying from 0.19 to 0.22. Hence, the Strouhal number can be used to approximately estimate the vortex shedding frequency. The vortex shedding frequency in Table 4 and the main frequency in Table 3 are also very close (the difference is less than 2%), so the Strouhal number can be used to predict the main frequency induced by the high-temperature steam as well.

3 Modal test of disc–stem assembly

In the above numerical simulations, the 3D unsteady flow in the full flow passage of the triple-eccentric butterfly valve was analyzed and the main frequencies of steam pressure fluctuation were obtained on both sides of the valve disc under different operating conditions. The pressure fluctuation of steam and the shedding of vortices can induce the vibration of the valve disc, where the fluid

Fig. 8 Pressure fluctuation frequency of Point 4, 5 and 8 at Section 0 for Cases 1 to 4: **a** Point 4; **b** Point 5; and **c** Point 8

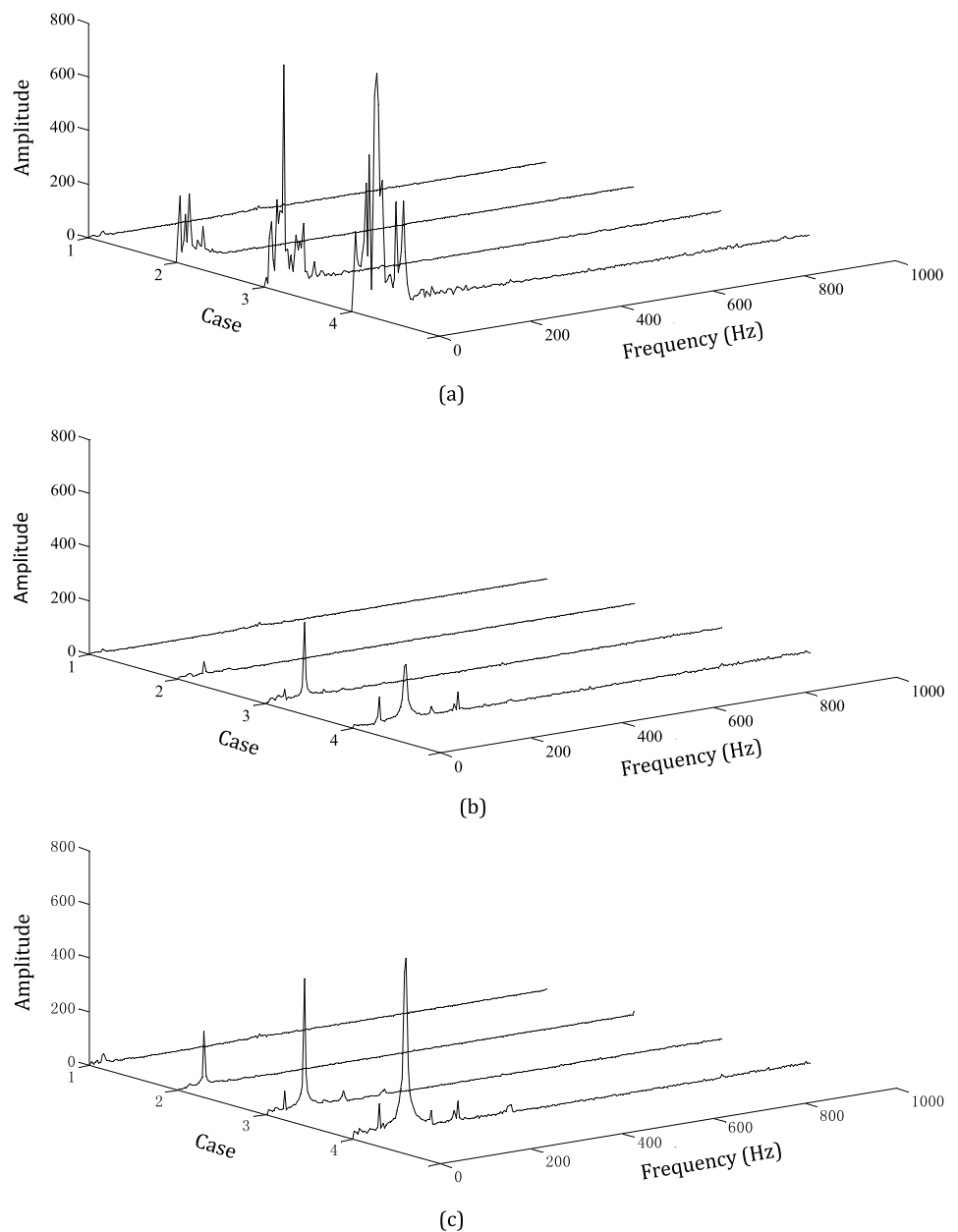


Table 4 Strouhal number and vortex shedding frequency

Case	Inflow velocity V (m/s)	Re	Vortex shedding frequency f_s (Hz)	Sr
1	18.10	2.98×10^6	31.5	0.22
2	36.42	6.00×10^6	58.6	0.21
3	54.63	9.00×10^6	80.5	0.19
4	72.84	1.20×10^7	115.0	0.21

force formed by the pressure fluctuation and the shedding of vortices comprise the external forces. When the fluid force frequency is close to the natural frequency of the disc–stem, resonance occurs. In order to judge whether

the disc–stem assembly resonates, an experimental modal test for the disc–stem assembly was conducted.

The natural frequency of the disc–stem assembly was measured by the hammering method in which the structure was excited by a force hammer. The hardware platform of this system consists of four parts: (a) exciter; (b) sensors; (c) data acquisition system; and (d) computer, which are shown in Fig. 9. The force hammer was connected directly to the signal-conditioning module of a DEWE5000 by a BNC connection. The impulse signal of the structure input was collected and transmitted to the computer for analysis. The response signal was connected to the amplifier through the acceleration sensor and then transformed by the DEWE5000. The signal was

Fig. 9 Modal analysis system: **a** exciter; **b** sensors; **c** data acquisition system; and **d** computer

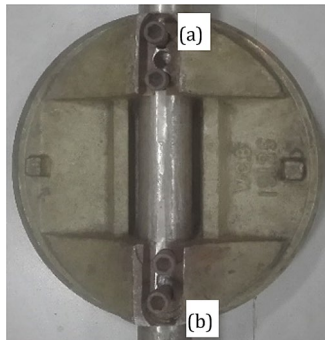


Fig. 10 Stem completely constrained with bolts: **a** the upper side; and **b** the lower side



Fig. 11 Modal test in progress

collected and stored by the frequency response analysis software, DEWEFRF.

According to actual operating conditions, the stem should be completely constrained as shown in Fig. 10. The stem was fixed on the triple-eccentric disc using four bolts. As shown in Fig. 11, when a force hammer impinges on the disc, the force hammer sends an impulse signal to the disc and then the computer processes the response signal and outputs the frequency characteristics as shown in Fig. 12.

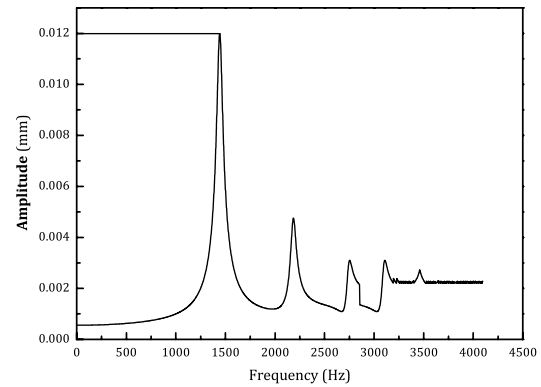


Fig. 12 Test results of frequency spectrum for disc-stem assembly

Analyzing the frequency characteristics in Fig. 12, there are five peaks in the characteristic curve, whose frequencies are 1443 Hz, 2186 Hz, 2755 Hz, 3147 Hz, and 3460 Hz. With increasing frequency, the peak value decreases gradually.

Compared with Table 3, in the maximum design flow rate Case 4, the maximum pressure fluctuation frequency was 117.2 Hz; but this was still much smaller than the 1443 Hz natural frequency of the disc-stem assembly. Therefore, it can be judged that the pressure fluctuation of fluid force does not induce resonance. In fact, in special engineering applications, the disc and stem are made of high-temperature and a greater density WC9 carbon steel; furthermore, the thickness of the disc and the diameter of the stem are both much greater than those in the conventional design. Therefore, the natural frequency of the disc assembly is relatively higher and there no lock-in phenomenon.

4 Conclusions

The pressure fluctuations induced by high-temperature steam flow through the stem-disc assembly inside a triple-eccentric butterfly valve was investigated by 3D unsteady flow simulation and experimental modal analysis. In the case of maximum flow rate, the main frequencies at Points 4 and 6 at Sections 0 were comparatively smaller than in other sections: 54.7 Hz and 103.5 Hz, respectively. Apart from these two points, the main frequencies at all other points in all sections were 117.2 Hz. The intensity at Point 4 in Sections 0 was clearly greatest.

As for different inlet flow rates, the study focused on the central section, Section 0. With increasing inlet flow rate, the main frequencies and amplitudes of pressure fluctuations at each point increased. Especially at Points 5 and 8, the steam fluctuation frequencies were 31.2, 58.6, 85.9, and 117.2 Hz, corresponding to the inlet mass flow rates

of 50, 100, 150, and 200 kg/s. The Strouhal numbers for the disc–stem assembly were about 0.19 to 0.21 for different flow rates.

The natural frequency of the disc–stem assembly obtained by the experimental modal analysis was 1443 Hz, which was much higher than the highest frequency (117.2 Hz) of steam pressure fluctuations in the case of maximum flow rate. Thus, the pressure fluctuation caused by the fluid force does not induce resonance of the disc–stem and no lock-in phenomenon occurs.

Acknowledgements This work was supported by the National Natural Science Foundation of China (Grant No. 51106099), the Opening Foundation of Key Laboratory of Aerodynamic Noise Control (Grant No. ANCL201602), and the Shanghai Civil Military Integration Project (Grant No. 26, 2014). The authors wish to express their appreciations to Mr. Li Hai of SEC-KSB Nuclear Pumps and Valves Co., Ltd., and to Mr. Zhao Liqiang of the Jiangsu Shazhou Valve Co. Ltd., China.

Compliance with ethical standards

Conflict of interest The authors declare that they have no conflict of interest.

References

- Zung P-S, Perng M-H (2002) Nonlinear dynamic model of a two-stage pressure relief valve for designers. *J Dyn Syst Meas Control Trans ASME* 124(1):62–66. <https://doi.org/10.1115/1.1435363>
- Smith BAW, Luloff BV (2000) The effect of seat geometry on gate valve noise. *J Press Vessel Technol Trans ASME* 122(4):401–407. <https://doi.org/10.1115/1.1286031>
- Jauvtis N, Williamson CHK (2004) The effect of two degrees of freedom on vortex-induced vibration at low mass and damping. *J Fluid Mech* 509:23–62. <https://doi.org/10.1017/s0022112004008778>
- Govardhan RN, Williamson CHK (2006) Defining the ‘modified Griffin plot’ in vortex-induced vibration: revealing the effect of Reynolds number using controlled damping. *J Fluid Mech* 561:147–180. <https://doi.org/10.1017/s0022112006000310>
- Facchinetti ML, de Langre E, Biolley F (2004) Coupling of structure and wake oscillators in vortex-induced vibrations. *J Fluids Struct* 19(2):123–140. <https://doi.org/10.1016/j.jfluidstruct.2003.12.004>
- Guilmineau E, Queutey P (2004) Numerical simulation of vortex-induced vibration of a circular cylinder with low mass-damping in a turbulent flow. *J Fluids Struct* 19(4):449–466. <https://doi.org/10.1016/j.jfluidstruct.2004.02.004>
- Mehmood A, Abdelkefi A, Hajj MR, Nayfeh AH, Akhtar I, Nuhait AO (2013) Piezoelectric energy harvesting from vortex-induced vibrations of circular cylinder. *J Sound Vib* 332(19):4656–4667. <https://doi.org/10.1016/j.jsv.2013.03.033>
- Franzini GR, Bunzel LO (2018) A numerical investigation on piezoelectric energy harvesting from vortex-induced vibrations with one and two degrees of freedom. *J Fluids Struct* 77:196–212. <https://doi.org/10.1016/j.jfluidstruct.2017.12.007>
- Duan Yu, Revell Alistair, Sinha Jyoti, Hahn Wolfgang (2019) A computational fluid dynamics (CFD) analysis of fluid excitations on the spindle in a high-pressure valve. *Int J Press Vessels Pip* 175:103922. <https://doi.org/10.1016/j.ijpvp.2019.103922>
- Govardhan R, Williamson CHK (2000) Modes of vortex formation and frequency response of a freely vibrating cylinder. *J Fluid Mech* 420:85–130. <https://doi.org/10.1017/s0022112000001233>
- Khalak A, Williamson CHK (1999) Motions, forces and mode transitions in vortex-induced vibrations at low mass-damping. *J Fluids Struct* 13(7–8):813–851. <https://doi.org/10.1006/jfls.1999.0236>
- Shoshani O (2018) Deterministic and stochastic analyses of the lock-in phenomenon in vortex-induced vibrations. *J Sound Vib* 434:17–27. <https://doi.org/10.1016/j.jsv.2018.07.023>
- Domnick CB, Benra F-K, Brillert D, Dohmen HJ, Musch C (2017) Investigation on flow-induced vibrations of a steam turbine inlet valve considering fluid-structure interaction effects. *J Eng Gas Turbines Power* 139(2):1. <https://doi.org/10.1115/1.403435>
- Galbally D, Garcia G, Hernando J, Sanchez JD, Barral M (2015) Analysis of pressure oscillations and safety relief valve vibrations in the main steam system of a boiling water reactor. *Nucl Eng Des* 293:258–271. <https://doi.org/10.1016/j.nucengdes.2015.08.005>
- Kumagai K, Ryu S, Ota M, Maeno K (2016) Investigation of poppet valve vibration with cavitation. *Int J Fluid Power* 17(1):15–24. <https://doi.org/10.1080/14399776.2015.1115648>
- Potter M, Bacic M (2012) Design and control of hardware-in-the-loop simulations for testing non-return-valve vibrations in air systems. *IEEE Trans Control Syst Technol* 20(1):98–110. <https://doi.org/10.1109/tcst.2011.2112660>
- Youn C, Asano S, Kawashima K, Kagawa T (2008) Flow characteristics of pressure reducing valve with radial slit structure for low noise. *J Vis* 11(4):357–364. <https://doi.org/10.1007/bf03182204>
- Wang H, Kong X, Liu H (2018) Vibration characteristics analysis for a tri-eccentric butterfly valve. *Zhendong yu Chongji/J Vib Shock* 37(5):202–206 and 212. <https://doi.org/10.13465/j.cnki.jsv.2018.05.030>

Publisher’s Note Springer Nature remains neutral with regard to jurisdictional claims in published maps and institutional affiliations.